TIME DOMAIN SIMULATION OF LARGE AMPLITUDE MOTIONS IN SHALLOW WATER

Amitava Guha, Abhilash Somayajula and Jeffrey Falzarano

Marine Dynamics Laboratory, Department of Ocean Engineering, Texas A&M University, Texas, USA,77843-3136

Proceedings of the 21st Offshore Symposium, February 2016, Houston, Texas
Texas Section of the Society of Naval Architects and Marine Engineers

ABSTRACT

A finite depth 3D Green function has been developed to estimate wave loads on the floating body in frequency domain which is then coupled with a time domain motion simulation tool. Nonlinear hydrostatic and Froude-Krylov forces have been incorporated considering the instantaneous wetted surface and the nonlinear equation of motion is then solved considering the large-amplitude rotations of the body. However, the option of using a consistent second order forcing model is also retained in the code where the linear diffraction forces and moments are augmented with the drift forces calculated from Newman approximation of difference frequency quadratic transfer functions (QTF).

The main advantage of the method lies in its capability to simulate large-amplitude motions of ship shaped and non-ship shaped vessels with or without mooring and with or without forward speed in deep or shallow water depths. This allows investigation of various nonlinear effects and ensures safe operation. It is particularly useful in modelling the motions of a ship in a port channel or towing of offshore platforms from fabrication yard to deep water installation site.

In this article, a methodical approach in validating the numerical results against published and other established numerical programs is presented for the developed finite depth Green function and hydrodynamic coefficient predictions. Also the drift forces and moments obtained by different forms of the Newman approximation are compared and validated against commercially available software. The ability of the time domain simulation program to capture nonlinearities is also shown by simulating the Mathieu type instability in heave and pitch modes of a Single Column Floater.

Keywords: Time domain, Shallow Water, Forward Speed, Large Amplitude, Hydrodynamics, Motion Simulation, Parametric Excitation, Single Column Floater

1 INTRODUCTION

Hydrodynamic wave excitation force and motion prediction using potential theory is a common practice in the marine and offshore industry. With the growing interest in renewable resources, the offshore wind and hydro kinetic energy extraction methods are being engineered applying similar techniques. Consideration of the finite depth effect and nonlinear forces are of critical importance in designing mooring systems and determining safe operational conditions which directly impacts the downtime.

A 3D Green function based potential theory method has been developed to obtain hydrodynamic coefficients and motion in frequency domain (Guha, 2012; Guha and Falzarano, 2015a). This method facilitates a quick analysis using discretized wetted surface of a vessel without modeling the water surface or other boundaries. A new finite depth Green function is developed and incorporated in this potential code to assess the effect of water depth on hydrodynamic coefficients. As the computational time for a numerical finite depth Green function has significant effect on the frequency domain analysis time, efficient algorithms bases on Newman (1990), Linton (1999), Pidcock (1985), Li (2001) and Liu et al. (2015) are implemented. In addition, the forward speed approximations using encounter frequency is also incorporated to simulate vessels traveling with nonzero forward speed in finite water depth.

Based on the frequency domain tool a time domain program has been developed to simulate the nonlinear equations of motion of a generalized floater. The developed tool includes the calculation of the nonlinear force vector including the nonlinear Froude-Krylov and hydrostatic forces and also is capable of handling large amplitudes of motion using an Euler angle consideration. In this paper two approaches of calculating the nonlinear force vector are described and their relative advantages and limitations are highlighted. The paper also demonstrates the application of both methods to two examples to demonstrate the importance of both methods. The first method is the calculation of nonlinear Froude-Krylov and hydrostatic force vector by integrating the pressure over the instantaneous underwater area under the incident wave. The second method is the more common approach of consideration of 2nd order forces using a quadratic transfer function (QTF) which is consistent upto second order. The second method is applied to the KCS container ship and its results are validated against the results from a commercially available software. Later the significant advantage of the first method is demonstrated by simulating the Mathieu type instability for the single column floater (SCF) which otherwise cannot be captured using a standard second order analysis. The SCF was originally suggested as a better alternative to classic spar (Huang et al., 2000) due to the advantages of wet towing to site and not requiring an upending for installation. However, it was later found that the Mathieu type instability was a major concern and the project was abandoned (Haslum, 2004). To avoid such scenarios, automated optimization techniques using evolutionary algorithms (Guha and Falzarano, 2015c) may be used to mitigate instability in the early design stage.

The time domain simulations also allow for a further statistical analysis which can help predict the extreme responses (Guha et al., 2013) and characterize its non-Gaussian probabilistic nature (Somayajula and Falzarano, 2014b).

2 FORMULATION

2.1 Estimation of wave excitation forces in finite water depth with or without forward speed

The fluid structure interaction forces on a floating body in a random sea is predicted by means of the principle of superposition. The random or irregular waves can be represented as a sum of constitutive regular waves and the linear forces on the floating body due to each regular wave can be summed together to obtain the total hydrodynamic force on the body. This leads to the frequency domain potential flow analysis where the wave induced forces are obtained for particular wave frequencies in an ideal fluid (incompressible, inviscid and irrotational).

To formulate the boundary value problem, a body (floating or fully submerged) is considered to be traveling with steady forward speed U or equivalently fixed in a current of equal magnitude and opposite direction. Regular wave of amplitude A, incidence frequency ω_I with heading angle β traveling in uniform water depth h is considered. The effect of finite water depth on wave frequency is expressed in terms of the dispersion relation $\omega^2 = kg\tanh(kh)$, where k is the wave number. An efficient code to solve the dispersion relation applying higher order iterative technique following Newman (1990) is developed.

The forward speed changes the frequency at which the body encounter the waves (Doppler effect), which is expressed as the encounter frequency $\omega_e = \omega_I - \frac{\omega_I^2}{g}U\cos\beta$. The unsteady fluid potential around the body is given by:

$$\Phi(\mathbf{x},t) = [-Ux + \phi_S(\mathbf{x})] + \left[\phi_I(\mathbf{x},\beta,\omega_I) + \phi_D(\mathbf{x},\beta,\omega_I) + \sum_{j=1}^{6}\eta_j\phi_j(\mathbf{x},U,\omega_e)\right]e^{i\omega_e t} \tag{2.1}$$

where ϕ_S is the steady disturbance potential due to forward motion of the body in calm water. ϕ_I is the potential due to incident wave, ϕ_D is the diffraction potential and ϕ_j is the radiation potential. η_j is the motion amplitude of the body in 6 degrees of freedom. Continuity condition in the fluid domain gives the Laplace equation:

$$\nabla^2\Phi = 0 \tag{2.2}$$

where the potential can be solved by applying following boundary conditions:

1. Combined dynamic and kinematic free surface boundary condition: $\left[\left(i\omega_e - U\frac{\partial}{\partial x}\right)^2 + g\frac{\partial}{\partial z}\right](\phi_I,\phi_D,\phi_j) = 0$ on $z = 0$
2. The bottom boundary condition: $\frac{\partial}{\partial z}(\phi_I,\phi_D,\phi_j) = 0 \qquad$ on $z = -h$
3. The Sommerfeld radiation condition: $\lim_{kr\to\infty}\sqrt{kr}\left(\frac{\partial}{\partial r} - ik\right)(\phi - \phi_I) = 0$
4. The body surface no-penetration boundary condition:
   (a) Radiation : $\frac{\partial\phi_j}{\partial n} = i\omega_e n_j + Um_j$ on S
   (b) Diffraction: $\frac{\partial\phi_I}{\partial n} + \frac{\partial\phi_D}{\partial n} = 0$ on S

where simplified $m_j \approx (0,0,0,0,n_3,-n_2)$ terms with body normal $\mathbf{n} = (n_1,n_2,n_3)$ are applied. The linear incident wave potential satisfying above boundary conditions is given by:

$$\phi_I = \frac{igA}{\omega_I}\frac{\cosh(k_I(z+h))}{\cosh(k_I h)}e^{-ik_I(x\cos\beta+y\sin\beta)} \tag{2.3}$$

The radiation potential in forward speed can be obtained using the zero speed potential as:

$$\phi_j = \phi_j^0 \qquad \text{for } j=1,2,3,4 \qquad\qquad \phi_5 = \phi_5^0 + \frac{U}{i\omega_e}\phi_3^0 \qquad\qquad \phi_6 = \phi_6^0 - \frac{U}{i\omega_e}\phi_2^0 \tag{2.4}$$

Analytical solution for the radiation potential ϕ_j and the diffraction potential ϕ_D are generally not available for arbitrary shaped bodies, which necessitates the use of numerical techniques such as the source distribution method.

2.1.1 The source distribution method

To obtain the diffraction and radiation velocity potentials, the body surface is discretized into N quadrilateral panels of area ΔS_j and an uniform source of unknown strength is distributed uniformly over each panel. The zero speed velocity potential can be written in terms of the unknown source strength σ as:

$$\phi^0 = \frac{1}{4\pi}\int_S \sigma(\mathbf{x}_s)G(\mathbf{x},\mathbf{x}_s)ds \tag{2.5}$$

where $\mathbf{x}$ is the field point where the potential is being evaluated due to a source at $\mathbf{x_s}$. Here, $G(\mathbf{x},\mathbf{x}_s)$ is the finite depth Green function which satisfies the free surface, bottom and radiation boundary conditions. Applying the body boundary condition gives:

$$-\frac{1}{2}\sigma_i + \frac{1}{4\pi}\sum_{j=1}^{N}\sigma(\mathbf{x}_s)\frac{\partial G}{\partial n}(\mathbf{x},\mathbf{x}_s)\Delta S_j = \begin{cases} i\omega_e n_j & : \text{Radiation} \\ -\dfrac{\partial \phi_I}{\partial n} & : \text{Diffraction} \end{cases} \tag{2.6}$$

This system of linear equations are solved using efficient matrix inversion algorithms to obtain the source strength σ_i on each panel.

2.1.2 The finite depth Green function

In obtaining the source strength on each panel of the body, the most computational burden is because of the Green function evaluation. For a body with N panels, the Green function must be evaluated for at least $(N-1)\times(N-1)$ times and 4 times this more in the case of a higher order integration method such as Gauss quadrature, which consumes a large portion of the CPU time. To overcome this, an efficient finite depth Green function has been developed. The analytical form of the finite depth Green function is given in John (1949, 1950) which is also summarized in Wehausen and Laitone (1960). In terms of numerical stability and the computational efficiency the finite depth Green function is divided into two separate functions which are used in the domain $R/h < 0.5$ and $R/h > 0.5$, where $R = \left[(x-\xi)^2 + (y-\eta)^2\right]^{1/2}$ is the horizontal distance from the source $q(\xi,\eta,\zeta)$ to the field point $p(x,y,z)$.

Integral form of the Green function

The integral form of the Green function is suitable for $R/h < 0.5$ and found to be unstable for $R/h > 7$. The analytical form of this function is given by Wehausen and Laitone (1960) as:

$$\begin{aligned} G(p;q) =& \frac{1}{r} + \frac{1}{r^*} \\ &+ 2PV\int_0^\infty \frac{(\mu+K)e^{-\mu h}\cosh(\mu(\zeta+h))cosh(\mu(z+h))}{\mu\sinh(\mu h) - K\cosh(\mu h)}J_0(\mu R)d\mu \\ &+ i\frac{2\pi(k+K)e^{-kh}\sinh(kh)\cosh(k(\zeta+h))\cosh(k(z+h))}{Kh+\sinh^2(kh)}J_0(kR) \end{aligned} \tag{2.7}$$

where

$$\begin{aligned} K =& \frac{\omega^2}{g} = k\tanh(kh) & r =& [(x-\xi)^2 + (y-\eta)^2 + (z-\zeta)^2]^{\frac{1}{2}} \\ r^* =& [(x-\xi)^2 + (y-\eta)^2 + (z+2h+\zeta)^2]^{\frac{1}{2}} & R =& [(x-\xi)^2 + (y-\eta)^2]^{\frac{1}{2}} \end{aligned} \tag{2.8}$$

The solution of the Rankine part for both source and the image source is obtained using the method described by Hess and Smith (1964). The full numerical implementation details for this is given in Guha (2012). The imaginary part of the Green function can be directly calculated. The numerical difficulty is presented mostly by the principal value integral part of the Green function. Using method of substitution the singularity of the function is removed and a form of that can be numerically integrated is obtained. The Gauss-Laguerre quadrature is implemented to obtain the integral value efficiently.

Series form of the Green function

The series form of the Green function is applicable for the rest of the domain $(R/h > 0.5)$. John (1949, 1950) derived the infinite series expansion for the finite depth Green function as:

$$\begin{aligned} G(p;q) =& 2\pi \frac{K^2-k^2}{k^2h-K^2h+K} \cosh(k(z+h))\cosh(k(\zeta+h))\,[Y_0(kR)+iJ_0(kR)]] \\ &+4\sum_{n=1}^{\infty} \frac{k_n^2+K^2}{k_n^2h+K^2h-K} \cos(k_n(z+h))\cos(k_n(\zeta+h))K(k_nR) \end{aligned} \tag{2.9}$$

where k_n denotes the set of corresponding positive real roots of equation: $k_n \tanh(k_nh) = -K$. Again, the function can be broken into real and imaginary parts. The imaginary part can be rewritten using the relation given by Wehausen and Laitone (1960) to be equal to the imaginary part of the integral form of the Green function which can be calculated directly. The real part of the Green function has a singularity at $R/h = 0$ and takes a significantly large number of terms in the infinite sum to give a converged solution. However, for the domain $R/h > 0.5$ a six decimal accuracy can be achieved by using approximately $6h/R$ number of terms. To be consistent, the algorithm is developed to iterate until a 7 significant digit accuracy is achieved.

A number of comparisons are made with published data to establish the validity of the code. Figure. 1 shows for the case $Kh = 5$ the comparison between the series and integral Green function with that of Li (2001) and Monacella (1966).

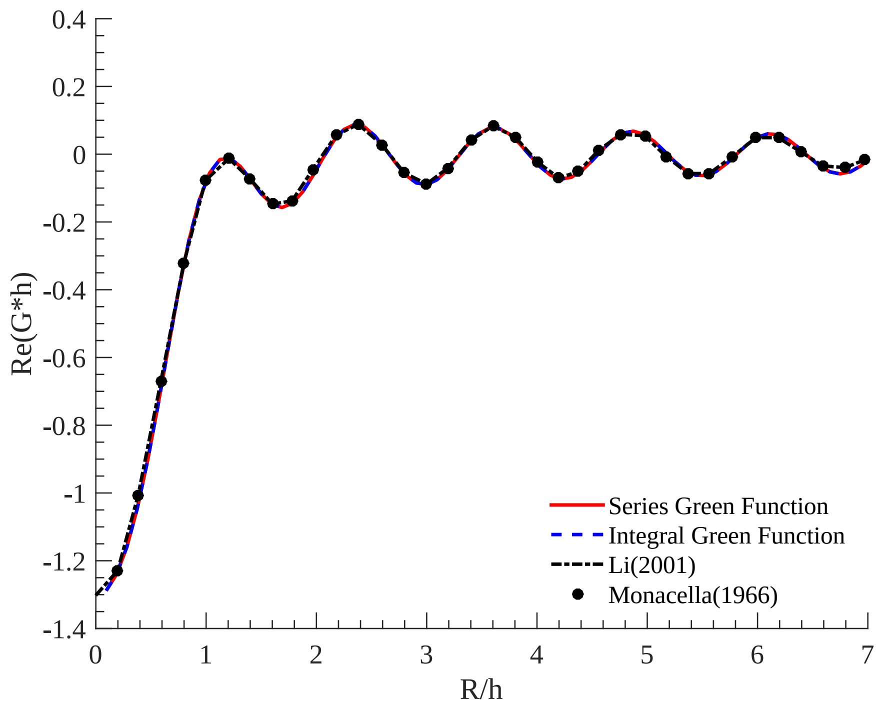

Figure. 1. The real part of Gh when $Kh = 5.0$, $kh = 5.000454$ and $0 < R/h < 7$

2.1.3 Forces and motions of the body

The forces and moments on the body are obtained by integrating the pressure over the submerged body surface. The pressure is obtained from the velocity potential by applying the Bernoulli's equation

$$P = \frac{1}{2}\rho U^2 - \rho\frac{\partial\Phi}{\partial t} - \frac{1}{2}\rho|\nabla\Phi|^2 - \rho g z \tag{2.10}$$

The hydrodynamic force can be obtained by:

$$F_{Hj} = -\int_S Pn_j ds \qquad j = 1,2,\ldots,6 \tag{2.11}$$

The added mass and damping is obtained by integrating the radiation pressure over the hull as:

$$A^0_{jk} = -\frac{\rho}{\omega_e}\int_S Im(\phi_k)n_j ds \qquad B^0_{jk} = -\rho\int_S Re(\phi_k)n_j ds \tag{2.12}$$

followed by forward speed corrections as described in Guha and Falzarano (2015a). The wave excitation force due to incident wave also known as the Froude-Krylov force is obtained as:

$$F_I = i\omega_I\rho\int_S \phi_I n_j ds \tag{2.13}$$

and the force due to diffracted wave is:

$$\begin{aligned}
F_D &= \rho\int_S (i\omega_e n_j - Um_j)\phi_D ds \\
&= -\rho\int_S \phi^0_j\frac{\partial\phi_I}{\partial n}ds \qquad \text{for } j = 1,2,3,4 \\
&= -\rho\int_S \phi^0_j\frac{\partial\phi_I}{\partial n}ds + \frac{\rho U}{i\omega_e}\int_S \phi^0_3\frac{\partial\phi_I}{\partial n}ds \qquad \text{for } j = 5 \\
&= -\rho\int_S \phi^0_j\frac{\partial\phi_I}{\partial n}ds - \frac{\rho U}{i\omega_e}\int_S \phi^0_2\frac{\partial\phi_I}{\partial n}ds \qquad \text{for } j = 6
\end{aligned} \tag{2.14}$$

The calculated added mass, damping and wave excitation forces are used to solve the equation of motion to get the vessel response as:

$$\sum_{k=1}^{6}[-\omega_e^2(M_{jk}+A_{jk}) + i\omega_e B_{jk} + C_{jk}]\eta_k = F^I_j + F^D_j \qquad j = 1,2,\ldots,6 \tag{2.15}$$

where M_{jk} is the mass matrix, C_{jk} is the hydrostatic stiffness matrix and η_k the vessel response in k^{th} mode of motion.

2.2 Time domain simulation considering large amplitude motion

The equations of motion describing a floating body are in general nonlinear and time varying. The fully nonlinear equations of motion of a general body have been derived in a variety of references including Abkowitz (1969), Lewandowski (2004), Somayajula and Falzarano (2015a) etc. In the vectorized form the equations of motion are given by

$$m[\ddot{\boldsymbol{\xi}} + \dot{\boldsymbol{\omega}}\times(\boldsymbol{x_G}-\boldsymbol{\xi}) + \boldsymbol{\omega}\times[\boldsymbol{\omega}\times(\boldsymbol{x_G}-\boldsymbol{\xi})]] = \boldsymbol{F} \tag{2.16}$$

$$I\dot{\boldsymbol{\omega}}' + \boldsymbol{\omega}'\times I\boldsymbol{\omega}' = R[\boldsymbol{M} - \boldsymbol{x_G}\times\boldsymbol{F}] \tag{2.17}$$

where m is the mass of the vessel, I is the moment of inertia matrix, $\boldsymbol{\xi}$ is the 3×1 vector representing the translational displacement vector, $\boldsymbol{x}_G$ represents the position vector of center of gravity in the inertial frame of reference, $\boldsymbol{\omega}$ and $\boldsymbol{\omega}'$ represent the angular velocity in the inertial frame of reference and body fixed frame respectively. $\boldsymbol{F}$ and $\boldsymbol{M}$ denote the external force and moment applied to the ship system. The detailed derivation of the equations of motion can be found in Somayajula and Falzarano (2015b). However, if nonlinearities due to inertial coupling are neglected, then theses equations can be reduced to the form shown in (2.15) for the case of a single regular incident wave.

In order to solve for the nonlinear equations of motion for corresponding motions, the nonlinear force and moment vectors need to be evaluated. The external forces and moments can be combined into a single 6×1 vector F and can be expressed as the sum of forces due to incident Froude Krylov $\{F_I\}$, scattering $\{F_S\}$, radiation $\{F_{Rad}\}$, viscous $\{F_V\}$ and restoring forces $\{F_{Res}\}$ as shown in (2.18).

$$\{F\} = \begin{Bmatrix}\boldsymbol{F}\\ \boldsymbol{M}\end{Bmatrix} = \{F_I\} + \{F_S\} + \{F_{Rad}\} + \{F_V\} + \{F_{Res}\} \tag{2.18}$$

The scattering and radiation forces are assumed to be linear and obtained using the frequency domain formulation described in section 2.1. While the scattering forces in the frequency domain are transformed into time domain using a Fourier transform, the radiation forces are more involved. In the frequency domain the radiation forces are expressed in terms of the frequency dependent added mass and radiation damping and are given by (2.19).

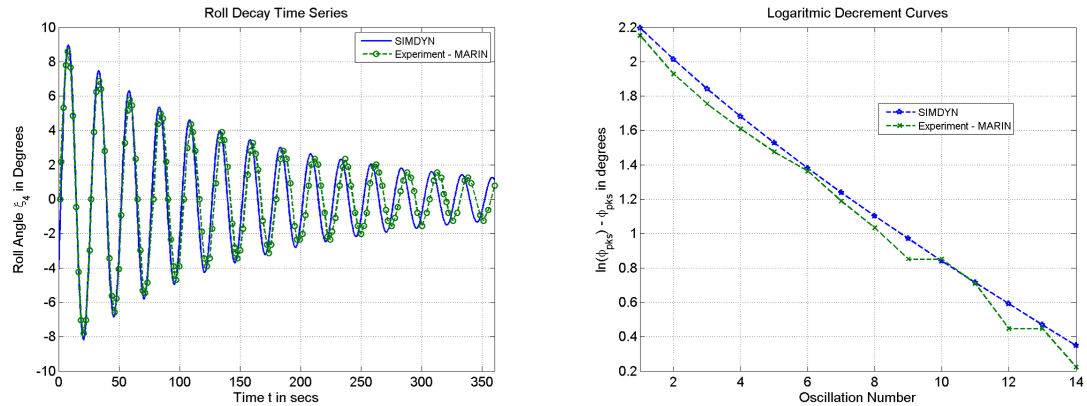

(a) Roll Decay Test

(b) Roll Decrement Curve

Figure. 2. Comparison of roll decay test from numerical simulation with experiments

$$\{F_{Rad}\} = -[A(\omega)]\{\ddot{\xi}\} - [B(\omega)]\{\dot{\xi}\} \tag{2.19}$$

However, in the time domain they are represented as a convolution integral given by (2.20) where $[K(\tau)]$ represents the 6×6 impulse response function (IRF) matrix. The IRFs $[K(\tau)]$ are related to the frequency dependent radiation damping $[B(\omega)]$ and can be obtained using (2.21). For more details on the numerical implementation of IRF calculation and calculation of the convolution integral please refer to Somayajula (2015).

$$\{F_{Rad}\} = -[A(\infty)]\{\ddot{\xi}\} - [B(\infty)]\{\dot{\xi}\} - \int_{-\infty}^{t} [K(t-\tau)]\{\dot{\xi}(\tau)\} d\tau \tag{2.20}$$

$$[K(\tau)] = \frac{2}{\pi} \int_0^{\infty} [B(\omega) - B(\infty)] \cos(\omega\tau) d\omega \tag{2.21}$$

While the scattering and radiation forces are considered to be linear, the developed simulation tool allows for the consideration of both linear and nonlinear Froude-Krylov and hydrostatics depending on user's choice. Two approaches are implemented here for considering nonlinearities due to Froude Krylov and hydrostatics. The first approach involves using the standard stretching formulation proposed by Wheeler (1970) where the linear wave kinematics are stretched to the instantaneous incident wave elevation and the corresponding pressure due to the stretched kinematics is integrated around the hull to give the nonlinear force vector at each time step (Somayajula and Falzarano, 2015a,b). This approach is necessary for simulating phenomenon which violate the assumption of small amplitude of motion utilized by linear theory, for example parametric excitation described in section 4.

The second approach is to use a consistent second order potential theory, which result in the capture of sum and difference frequency forces arising from a bi-chromatic incident waves. The resulting second order forces and moments are usually an order of magnitude smaller than the linear theory forces and moments and play a significant role when the natural frequency of the vessel being analyzed is outside the wave frequency zone (which is a typical case for offshore structures). Details of calculating the second order drift forces are discussed in section 2.3. It is however, important to note that including nonlinear Froude-Krylov and hydrostatic forces due to Wheeler stretching should not be used in conjunction with second order drift forces as it results in double counting the non-linearities.

The viscous damping force is obtained by the standard approach suggested by Ikeda et al. (1978) which separates the effective linear damping into its components - skin friction damping, wave damping, eddy damping, lift damping and bilge keel damping. Each of these components except the wave damping (obtained exactly from frequency domain analysis) are calculated using empirical relations. The empirical expressions are well documented in Falzarano et al. (2015). Figure. 2 shows a comparison of the roll decay test obtained from numerical simulation using empirical model with the experiments performed at MARIN for the Pram hull form. The comparison demonstrates that the empirical predictions work fairly well for a general ship shaped structure.

Once all the components of the force vector are evaluated, the differential equations (2.16) and (2.17) governing the of motion are solved using a 4^{th} order Runge-Kutta numerical integration scheme to obtain the nonlinear motions.

2.3 Calculation of the second order mean drift forces and the Quadratic Transfer Functions

The influence of second order mean drift forces are proven to be of critical importance in the prediction of stability criteria for floating bodies as well in determining the integrity of the mooring system design. Numerical prediction of the mean drift forces rely primarily upon two methods. First, the far field method proposed by Maruo (1960) which is based on diffracted and radiated wave energy and the momentum flux at infinity. Second is the near field method first proposed by Boese (1970) and later modified by Pinkster (1979) and Faltinsen et al. (1980). This method is more intuitive and gives forces in all 6DOF compared to the former which can only provide forces in 3DOF. In the near field method, a perturbation approach is applied to differentiate zeroth, first and second order quantities and the forces and moments are simply obtained by integrating the hydrodynamic pressure on the body surface.

2.3.1 Mean drift forces

The velocity potential ϕ, wave elevation ζ, relative wave elevation ζ_r, body motion amplitude η and the pressure p are perturbed using a small parameter ε of the order of the wave slope assuming small amplitude oscillation of the body about a mean position.

$$\begin{aligned} &\phi = \varepsilon\phi^{(1)} + \varepsilon^2\phi^{(2)} + \dots \qquad &&\zeta = \varepsilon\zeta^{(1)} + \varepsilon^2\zeta^{(2)} + \dots \qquad &&\zeta_r = \varepsilon\zeta_r^{(1)} + \varepsilon^2\zeta_r^{(2)} + \dots \\ &\eta = \varepsilon\eta^{(1)} + \varepsilon^2\eta^{(2)} + \dots &&p = p^{(0)} + \varepsilon p^{(1)} + \varepsilon^2 p^{(2)} + \dots \end{aligned} \tag{2.22}$$

Substituting above expressions into the Bernoulli's equation (2.10) gives the expression for zeroth, first and second order pressures. Similarly, the perturbation of the hydrodynamic force in equation (2.11) give:

$$\mathbf{F} = -\left(\int_{S_0} ds + \int_{wl} \zeta_r dl\right)\left(p^{(0)} + \varepsilon p^{(1)} + \varepsilon^2 p^{(2)}\right)\left(\mathbf{n}^{(0)} + \varepsilon(\theta^{(1)} \times \mathbf{n}^{(0)}) + \varepsilon^2 H\mathbf{n}^{(0)}\right) \tag{2.23}$$

Separating terms with ε^2 gives the second order force equation as:

$$\begin{aligned} \mathbf{F}^{(2)} = &-\int_{wl} \frac{1}{2}\rho g\left(\zeta_r^{(1)}\right)^2 \frac{\mathbf{n}^{(0)}}{\sqrt{1-n_3^2}} dl + \int_{S_0} \rho\left(\frac{\partial\phi^{(2)}}{\partial t} - U\frac{\partial\phi^{(2)}}{\partial x}\right)\mathbf{n}^{(0)} ds \\ &+ \int_{S_0} \frac{\rho}{2}\left\{\left(\frac{\partial\phi^{(1)}}{\partial x}\right)^2 + \left(\frac{\partial\phi^{(1)}}{\partial y}\right)^2 + \left(\frac{\partial\phi^{(1)}}{\partial z}\right)^2\right\}\mathbf{n}^{(0)} ds \\ &+ \int_{S_0} i\omega_e\rho\left\{(\eta_1 - \eta_6 y_B + \eta_5 z_B)\frac{\partial\phi^{(1)}}{\partial x}\right. \\ &\left. + (\eta_2 + \eta_6 x_B - \eta_4 z_B)\frac{\partial\phi^{(1)}}{\partial y} + (\eta_3 - \eta_5 x_B + \eta_4 y_B)\frac{\partial\phi^{(1)}}{\partial z}\right\}\mathbf{n}^{(0)} ds \\ &- \rho g A^{(0)}\left[\eta_4\eta_6 x_{B,f} + \eta_5\eta_6 y_{B,f} + \frac{1}{2}(\eta_4^2 + \eta_5^2)Z_0\right]\hat{k} \\ &- \omega_e^2\left\{-\eta_2\eta_6 m + \eta_4\eta_6 m z_g - \eta_6\eta_6 m x_g + \eta_3\eta_5 m + \eta_4\eta_5 y_g - \eta_5\eta_5 m x_g\right\}\hat{\imath} \\ &- \omega_e^2\left\{\eta_1\eta_6 m + \eta_5\eta_6 m z_g - \eta_6\eta_6 m y_g - \eta_3\eta_4 m - \eta_4\eta_4 m y_g + \eta_4\eta_5 m x_g\right\}\hat{\jmath} \\ &- \omega_e^2\left\{-\eta_1\eta_5 m - \eta_5\eta_5 m z_g + \eta_5\eta_6 m y_g + \eta_2\eta_4 m - \eta_4\eta_4 m z_g + \eta_4\eta_6 m x_g\right\}\hat{k} \end{aligned} \tag{2.24}$$

Taking a time average over one wave period cancels the term with the second order potential and the rest of the terms can be evaluated from the linear potential theory. Similarly the second order moment terms can be obtained, but excluded from here for brevity (See Guha (2016)). These forces are known as the mean drift forces.

2.3.2 Quadratic Transfer Functions

The second order force and moment obtained from perturbation theory accommodate interaction between two wave trains with different amplitudes and frequencies. The interaction between two regular waves (bi-chromatic waves) gives rise to forces and moments at difference and sum frequencies. The total second order force (given by (2.24)) and moment separated into components due to the sum and difference frequency effects as represented below.

$$\boldsymbol{F}^{(2)}(\omega_m, \omega_n) = \boldsymbol{F}^{(2d)}(\omega_m, \omega_n) + \boldsymbol{F}^{(2s)}(\omega_m, \omega_n) \tag{2.25}$$

$$\tag{2.26}$$

where $\boldsymbol{F}^{(2s)}(\omega_m,\omega_n)$ and $\boldsymbol{F}^{(2d)}(\omega_m,\omega_n)$ are the sum and difference frequency components of the second order force respectively. If the two regular wave trains in a bi-chromatic wave have amplitudes A_m and A_n, a set of second order transfer functions can be defined as shown below. These transfer functions are also referred to as quadratic transfer functions (QTFs).

$$Q_i^{(2d)}(\omega_m,\omega_n) = \frac{F_i^{(2d)}(\omega_m,\omega_n)}{A_m A_n} \qquad Q_i^{(2s)}(\omega_m,\omega_n) = \frac{F_i^{(2s)}(\omega_m,\omega_n)}{A_m A_n} \qquad \text{for } i = 1,2,3 \tag{2.27}$$

$$Q_i^{(2d)}(\omega_m,\omega_n) = \frac{M_{i-3}^{(2d)}(\omega_m,\omega_n)}{A_m A_n} \qquad Q_i^{(2s)}(\omega_m,\omega_n) = \frac{M_{i-3}^{(2s)}(\omega_m,\omega_n)}{A_m A_n} \qquad \text{for } i = 4,5,6 \tag{2.28}$$

For most of the offshore structures (except TLPs) such as spars, semi-submersibles and FPSOs, the difference frequency effects are significantly important than the sum frequency effects. It is practically observed that the largest contribution to the second order forces usually comes from frequency pairs which are close by ($\omega_m \approx \omega_n$). For such cases, Newman suggested an approximation to calculate the difference frequency QTF by using just the mean drift coefficients. The original approximation suggested by Newman is given by:

$$Q^{(2d)}(\omega_m,\omega_n) = Q^{(2d)}(\omega_m,\omega_m) \tag{2.29}$$

However, other forms of Newman approximation which have become quite accepted include the arithmetic mean and geometric mean models shown in (2.30) and (2.31) respectively.

$$Q^{(2d)}(\omega_m,\omega_n) = \frac{1}{2}\left(Q^{(2d)}(\omega_m,\omega_m) + Q^{(2d)}(\omega_n,\omega_n)\right) \tag{2.30}$$

$$Q^{(2d)}(\omega_m,\omega_n) = \operatorname{sign}(Q^{(2d)})\sqrt{Q^{(2d)}(\omega_m,\omega_m)Q^{(2d)}(\omega_n,\omega_n)} \tag{2.31}$$

The second order force in time domain is obtained by taking a double Fourier transform of the product of QTF with the pairs of harmonic amplitudes of the wave train and is shown in (2.32).

$$F_i^{(2d)}(t) = \operatorname{Re}\left\{\sum_{m=1}^{N}\sum_{n=1}^{N} A_m A_n^* Q_i^{(2d)}(\omega_m,\omega_n) e^{i(\omega_m-\omega_n)t}\right\} \tag{2.32}$$

where A_m and A_n represent the amplitudes of the m^{th} and n^{th} components of an irregular wave train given by (2.33).

$$\eta(t) = \operatorname{Re}\left\{\sum_{m=1}^{N} A_m e^{i\omega_m t}\right\} \tag{2.33}$$

However, there are more efficient ways to implement the above formulation numerically where instead of taking a double Fourier transform, the calculation can be reduced to a single Fourier transform over a series sum (Duarte and Sarmento, 2014; Somayajula, 2015).

3 VALIDATIONS

3.1 Finite depth calculations in frequency domain

The new finite depth Green function developed is incorporated in the frequency domain tool MDLHydroD (Guha (2012); Guha and Falzarano (2013, 2015a)). This enabled the program to be able to predict hydrodynamic loads and corresponding motion for submerged or floating bodies in deep and finite water depth with or without forward speed. The unique capability of consideration of the hull emergence angle in prediction of added resistance (Somayajula et al. (2014); Guha and Falzarano (2015b)) also becomes available for the finite waterdepth condition. A number of validation studies have been performed comparing calculated results with experimental as well as other commercially available numerical tools and found to be in good agreement.

Here, a truncated cylinder of radius 1m and draft 0.5m is considered. The water depth of 1m corresponds to the depth to draft ratio(h/T) of 2 is chosen. The vertical center of gravity is set at $z = 0$ and the radius of gyrations in roll, pitch and yaw are considered to be 1m. The frequency domain results are obtained for wave heading 150 degrees and zero forward speed. Figure. 3 shows the panel model of the cylinder. The calculated results are compared with an industry standard program (Lee (2013)). Figure. 4 - 7 shows the comparison of the response amplitude operators for surge, heave, roll and pitch mode of motions and Figure. 8 shows the

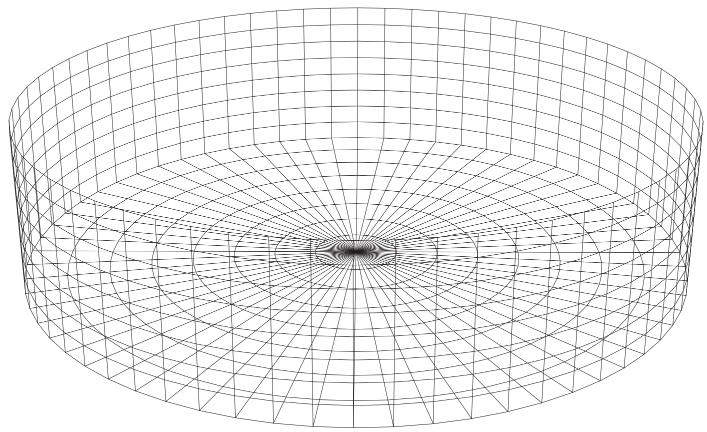

Figure. 3. Panel model of the cylinder

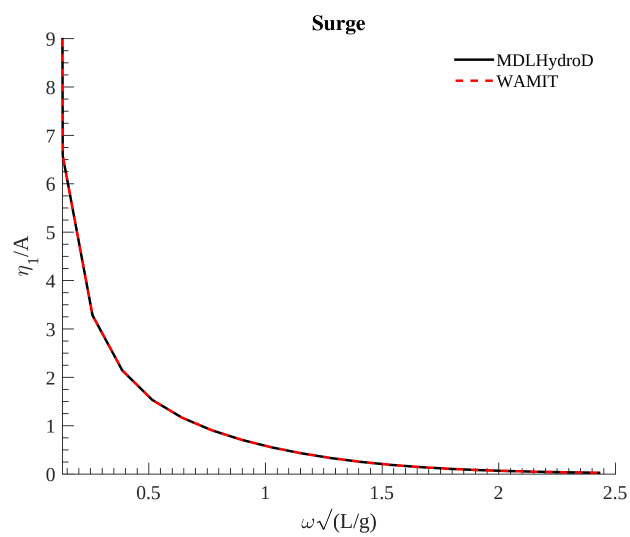

(a) Surge RAO amplitude

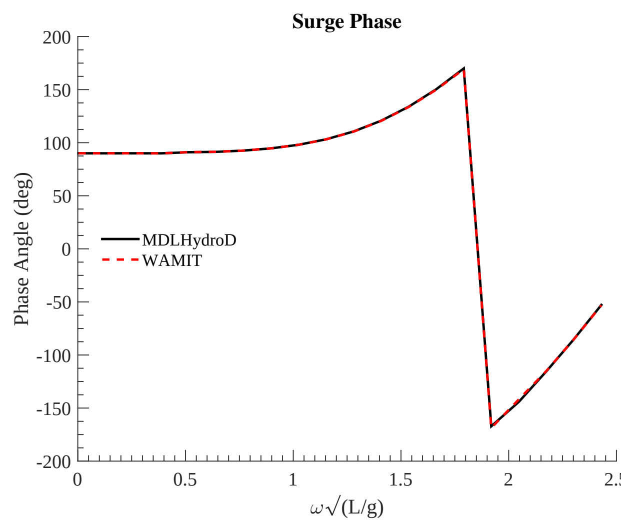

(b) Surge RAO phase

Figure. 4. Surge RAO comparison for cylinder at $Fn = 0$ and $h/T = 2$

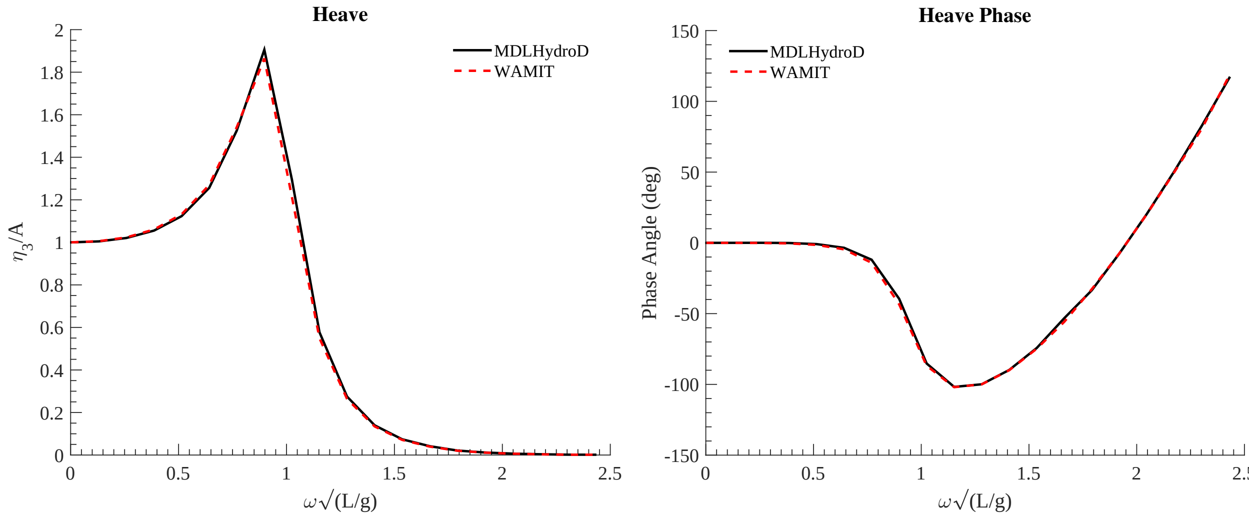

(a) Heave RAO amplitude

(b) Heave RAO amplitude

Figure. 5. Heave RAO comparison for cylinder at $Fn = 0$ and $h/T = 2$

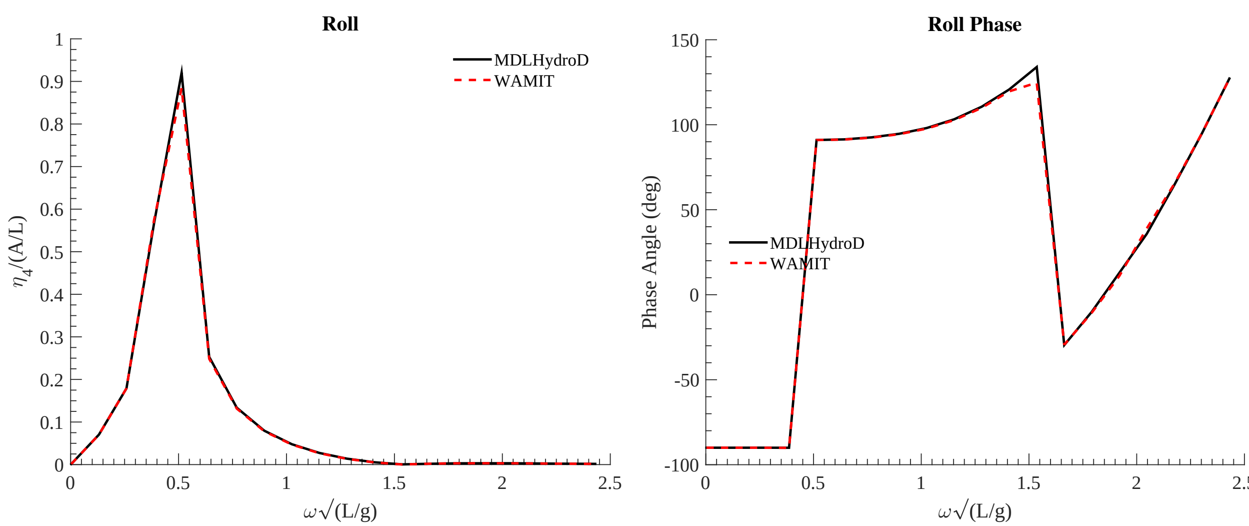

(a) Roll RAO amplitude

(b) Roll RAO phase

Figure. 6. Roll RAO comparison for cylinder at $Fn = 0$ and $h/T = 2$

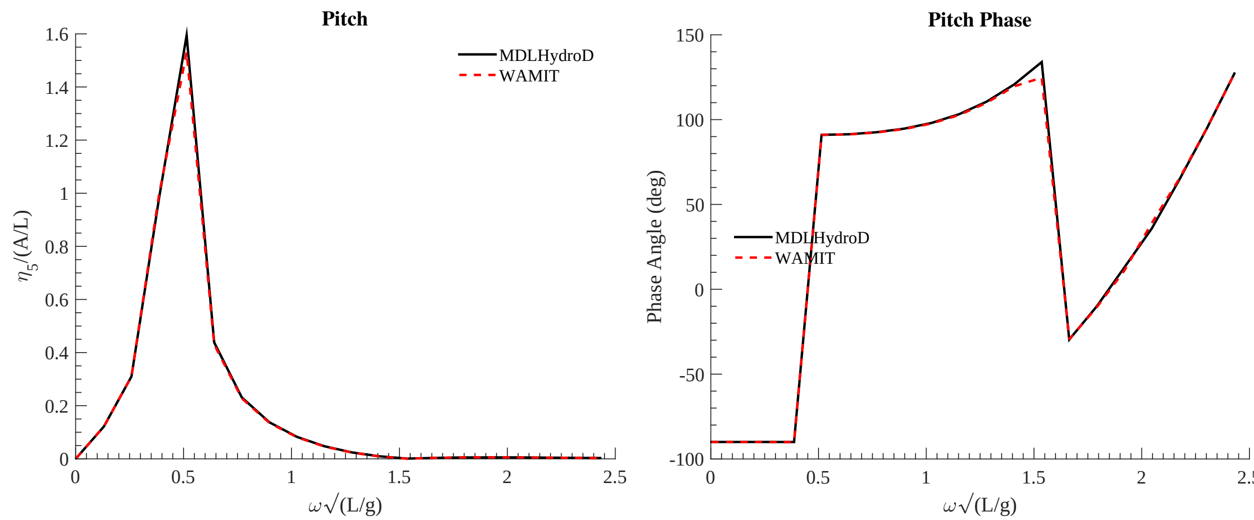

(a) Pitch RAO amplitude (b) Pitch RAO phase

Figure. 7. Pitch RAO comparison for cylinder at $Fn = 0$ and $h/T = 2$

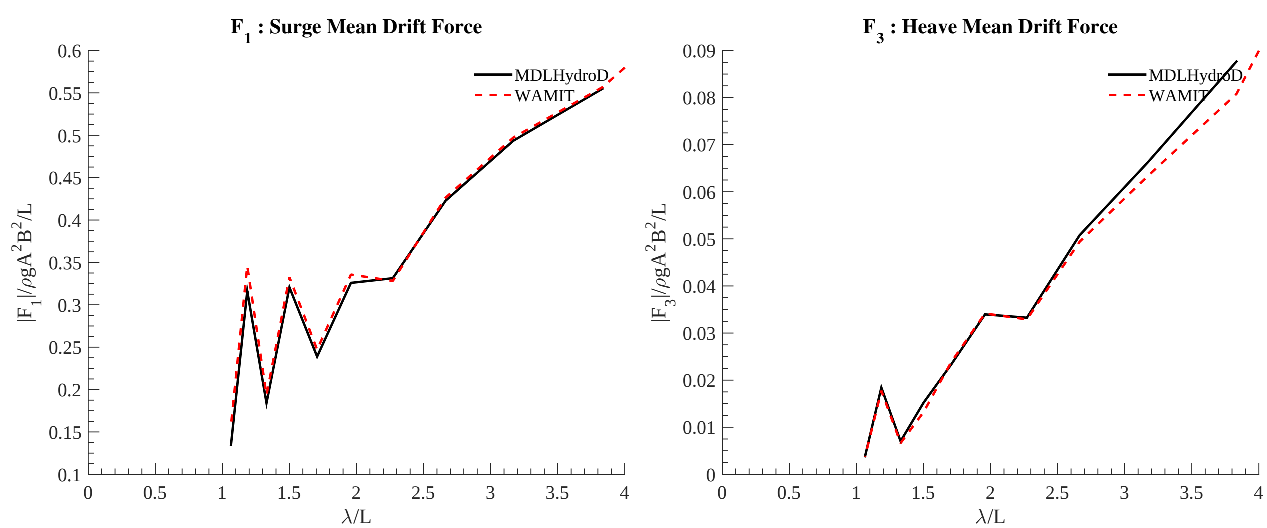

(a) Surge mean drift force (b) Heave mean drift force

Figure. 8. Comparison of mean drift forces for cylinder at $Fn = 0$ and $h/T = 2$

comparison of the mean drift force in surge and heave. In all of the cases, the results were found to be in excellent agreement with the industry standard code.

The finite depth forward speed motion prediction results are relatively scarce in the open literature. Here the added mass coefficients are compared in Figure. 9 with published results of Huijsmans, R.H.M. and Dallinga (1983) for the Series 60 hull with $C_b = 0.7$. The depth to draft ratio $h/T = 1.15$ is considered and forward speed corresponding to $Fn = 0.2$ is selected. The results were found to be satisfactory. Further validation results are presented in Guha (2016).

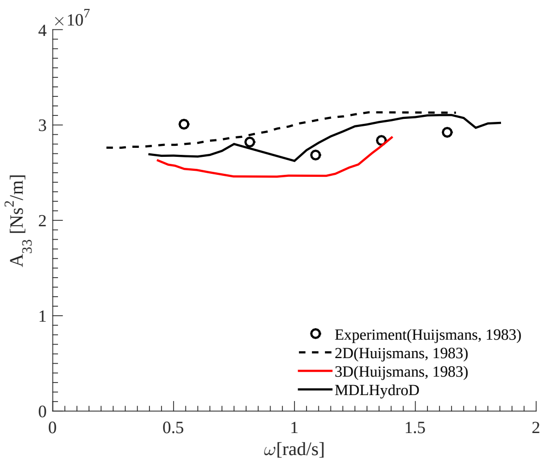

(a) A_{33}

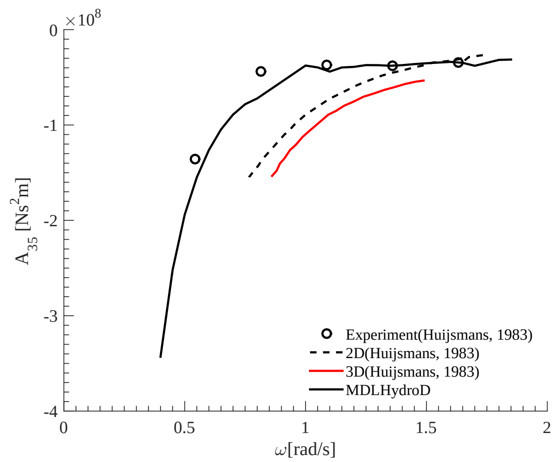

(b) A_{35}

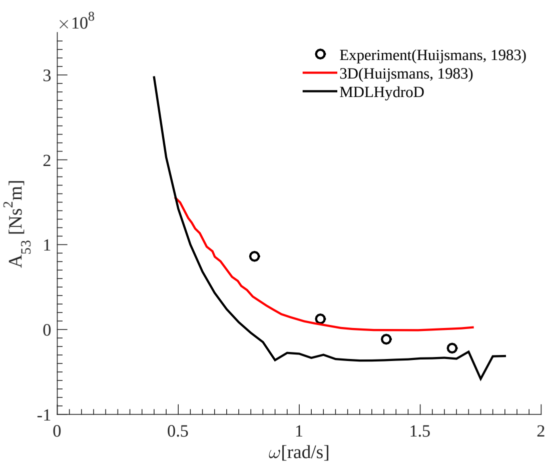

(c) A_{53}

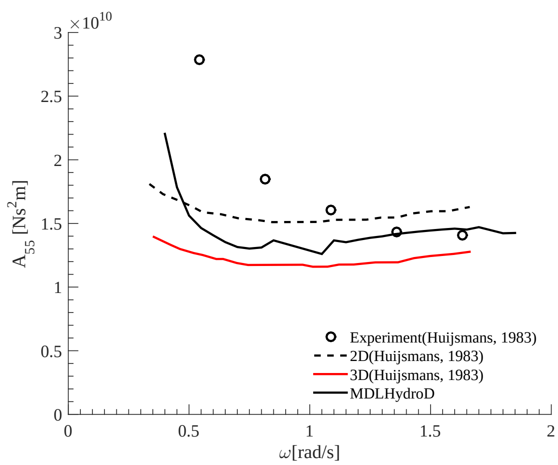

(d) A_{55}

Figure. 9. Comparison of added mass for Series 60 ($Cb = 0.7$) hull at $Fn = 0.2$ and $h/T = 1.15$

3.2 Time domain results

In addition to the frequency domain tool, an in-house time domain tool SIMDYN has also been developed to simulate the nonlinear equations of motion of a general floating body in time domain while including:

- Nonlinear Froude-Krylov forces
- Nonlinear hydrostatics
- Viscous forces and moments

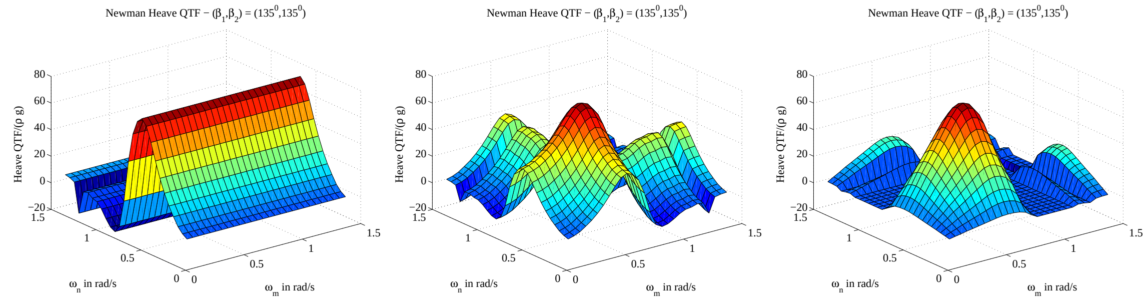

(a) Original (b) Arithmetic Mean (c) Geometric Mean

Figure. 11. Heave QTF using different Newman approximations

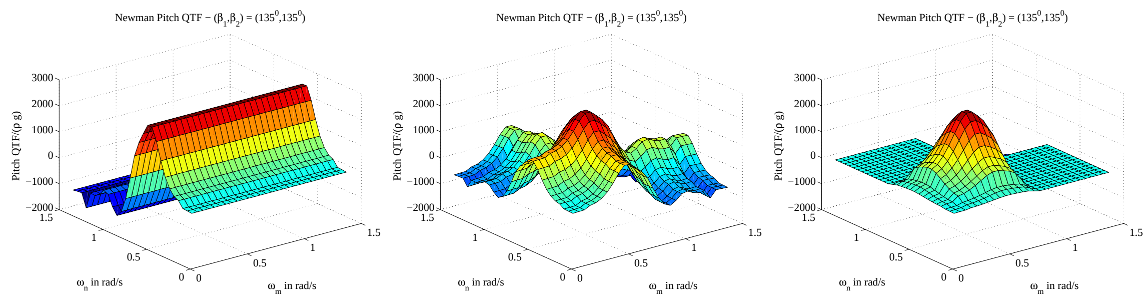

(a) Original (b) Arithmetic Mean (c) Geometric Mean

Figure. 12. Pitch QTF using different Newman approximations

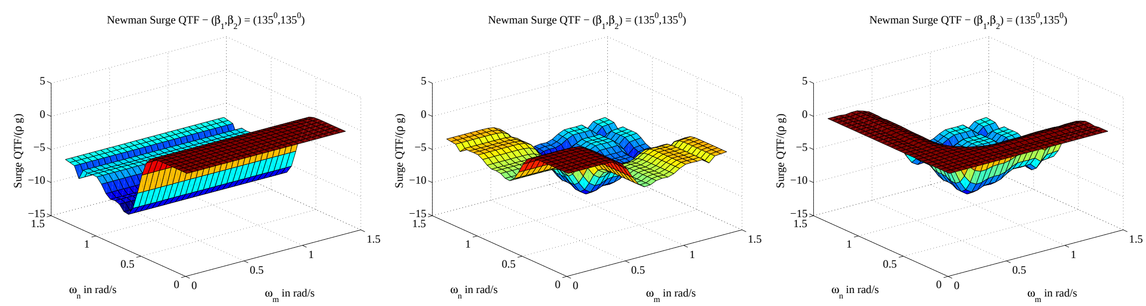

(a) Original (b) Arithmetic Mean (c) Geometric Mean

Figure. 10. Surge QTF using different Newman approximations

Similar to the frequency domain tool, the time domain simulation program has also been extensively validated against experimental data and other existing commercial codes. Figure. 10, Figure. 11 and Figure. 12 shows the surge, heave and pitch QTFs computed using different forms of the Newman approximation for the KCS container ship (hull form publicly available).

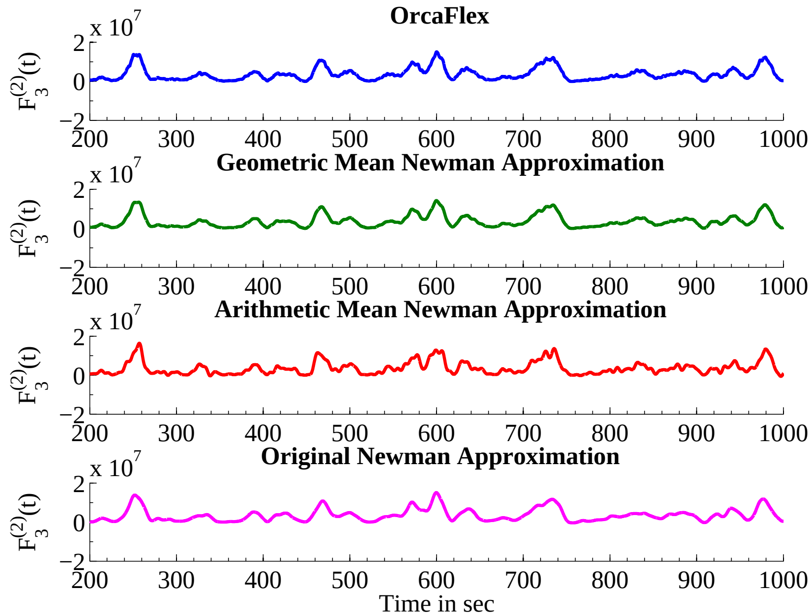

Figure. 14. Comparison of 2^{nd} order heave force in time domain

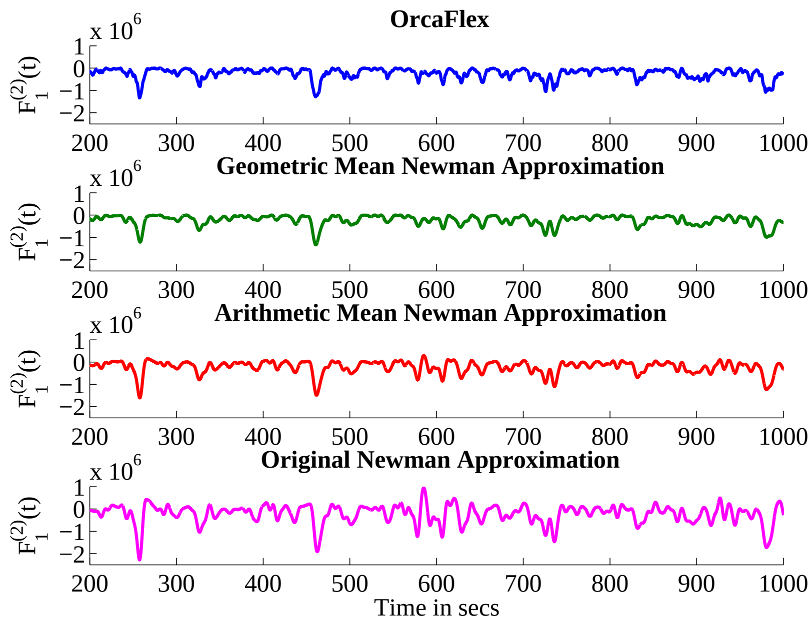

Figure. 13. Comparison of 2^{nd} order surge force in time domain

The corresponding second order surge force, heave force and pitch moment in time domain have been compared against the results from the commercially available software OrcaFlex (Orcina, 2015) and are shown in Figure. 13, Figure. 14 and Figure. 15 respectively. It is important to note that OrcaFlex uses the geometric mean Newman approximation to calculate the second order drift forces and moments. It can be seen from the comparisons that the second order forces and moments obtained by geometric mean Newman approximation in the current study agree well with the the results obtained from OrcaFlex.

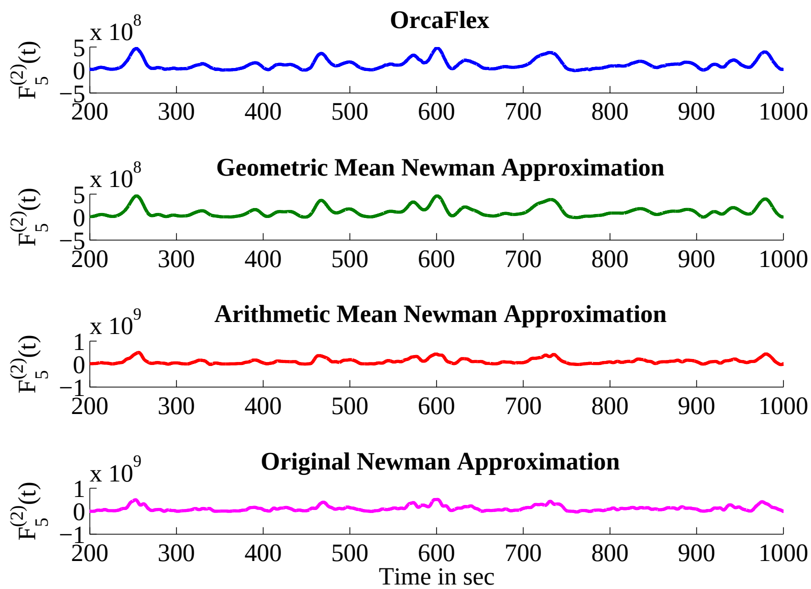

Figure. 15. Comparison of 2^{nd} order pitch moment in time domain

4 PARAMETRIC EXCITATION IN SINGLE COLUMN FLOATER

While the previous section demonstrated the application of the frequency and time domain tool using a consistent second order formulation, this section demonstrates an application of the nonlinear time domain simulation while including the nonlinear Froude-Krylov and hydrostatics using a Wheeler stretched kinematics. It is reiterated that the Wheeler stretched approach although not order consistent is very robust in simulating instabilities experienced by ships and offshore platforms, especially involving parametric excitation which cannot be captured using the second order approach.

Parametric excitation is characterized by a large amplitude of motion even when the direct exciting force is close to zero. In general, it is caused due to a time varying parameter of the system such as stiffness or damping. It has recently been observed to be a serious concern for container ships in both regular (Moideen et al., 2012, 2013) and irregular waves (Moideen et al., 2014; Somayajula and Falzarano, 2014a; Somayajula et al., 2014). However, recent studies by Haslum et al. (1999); Haslum (2000) have shown that even certain offshore platforms such as classic spars and single column floaters are susceptible to parametric excitation.

In this section we demonstrate this effect for a single column floater (SCF) originally proposed by ABB (Huang et al., 2000). A rendered surface model of the SCF is shown in Figure. 16 and its particulars are listed in Table 1. The SCF includes a moonpool through both the hard tank and the soft tank and its details can be found in Chou et al. (2004). The moonpool has been considered while simulating the motions numerically. As the objective of this study is to demonstrate that the discussed simulation tool is able to capture the dynamics of instability, the truss elements connecting the two tanks (which provide quite a bit of damping) are not included in the numerical model. For a detailed drawing describing the dimensions please refer to Chou et al. (2004).

Table 1. Particulars of the Single Column Floater

Particulars	Values
Draft (m)	62.48
Displacement (tonnes)	38507.54
Freeboard (m)	12.19
KG (m)	20.88
Roll and Pitch Radius of Gyration (m)	45.47

4.1 Critical frequency for parametric excitation

The parametric instability in spar type platforms is exhibited as a response amplification in the coupled heave and pitch modes. For a clearer understanding, lets consider a spar platform being excited by regular waves with a frequency ω different from the natural

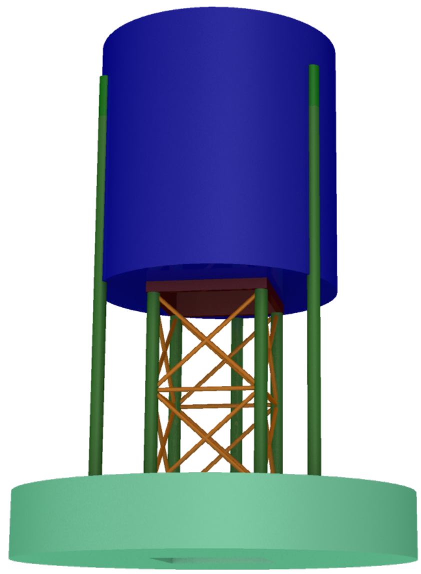

Figure. 16. Single Column Floater

heave frequency ω_{n3}. Due to the low damping in heave mode of motion the heave response is composed of the superposition of the steady state motion at wave frequency ω and the transient motion at heave natural frequency ω_{n3}. The superposition of the transient response with the steady state motion leads to a heave response envelope oscillating with frequency $|\omega - \omega_{n3}|$. Haslum (2000) showed that if the frequency associated with the envelope of the heave motion coincides with the pitch natural frequency $\omega - \omega_{n3} = \omega_{n5}$, the system experiences as parametric excitation in pitch mode of motion.

$$\omega_{n5} = \omega - \omega_{n3} \tag{4.1}$$

The critical wave period at which this effect is seen can be expressed in terms of the heave and pitch natural periods and is given by:

$$T_{\text{critical}} = \frac{2\pi}{\omega} = \frac{2\pi}{\omega_{n3} + \omega_{n5}} = \frac{1}{\frac{1}{T_{n3}} + \frac{1}{T_{n5}}} \tag{4.2}$$

However, it is also clear that the difference frequency between the incident wave and Mathieu excited pitch motion coincides with the heave natural frequency which leads to a resonant amplification of the heave motion. The resonant heave motion leads to a larger amplitude of heave envelope process which feeds back into the Mathieu pitch motion and the cycle continues.

4.2 Simulation of instability for SCF

The time domain simulation tool developed in subsection 2.2 is applied to simulate the motions of the single column floater in both regular and irregular waves. Figure. 17 and Figure. 18 show the comparisons of heave and pitch responses from the nonlinear simulation with linear theory. Note that the motions are specified about an origin located at the center of gravity of the vessel. It can be seen that both the heave and the pitch motions show an exponential rise from the steady state linear solution which is also a charecteristic exhibited by parametric response.

5 CONCLUSIONS

A new efficient finite water depth Green function has been developed and incorporated in a 3D potential flow solver. The paper presents key expressions used in developing the numerical finite depth Green function and compares with published results. The

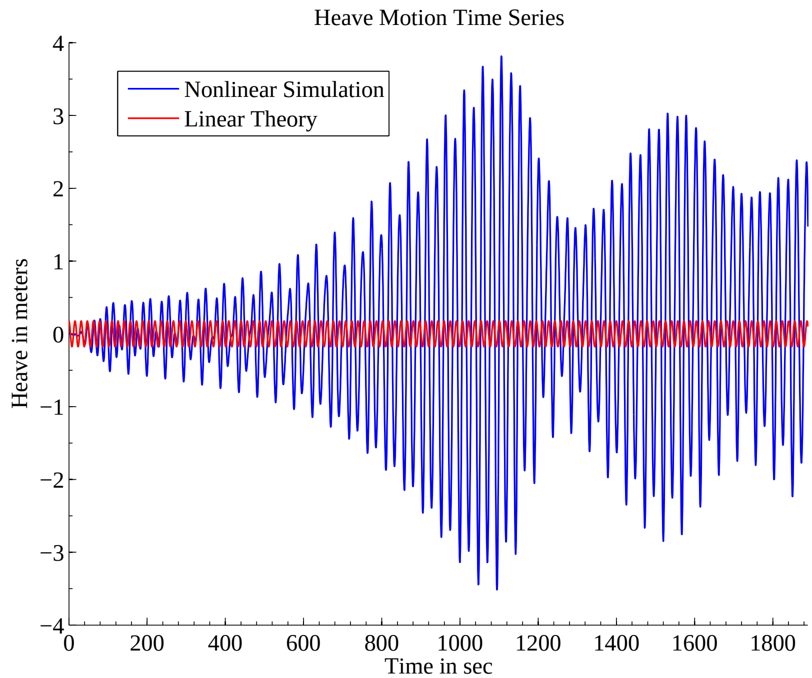

Figure. 17. SCF heave response in regular waves with $H = 8\ m$ and $T = 15.73\ s$

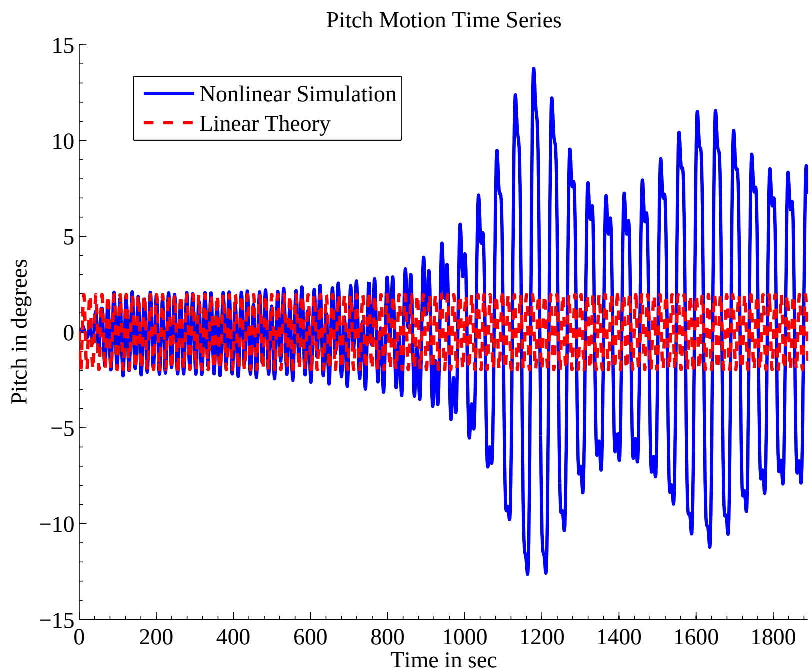

Figure. 18. SCF pitch response in regular waves with $H = 8\ m$ and $T = 15.73\ s$

motion prediction for a floating cylinder at shallow water depth is compared with results obtained from a commercial software. Furthermore, the hydrodynamic coefficients at forward speed in finite water depth is also presented for a ship shaped structure.

The paper also discusses the development of a nonlinear time domain simulation tool to simulate the nonlinear motions of a generalized floater. Two specific approaches to calculate the nonlinear force vector are discussed along with examples. It is shown that both the approaches of calculating the nonlinear force and moment vectors - stretching kinematics and second order analysis - are needed to allow for simulation of the various phenomena observed in marine and offshore structure analysis. The second order model has been validated against a commercially available software. The developed tool has also been specifically applied to the problem of Mathieu type instability in SCFs to demonstrate that the simulation program is able to capture the relevant dynamics of the system. While the two approaches are applicable to different types of problems, the option of having a combination of the two approaches allows for a strong hydrodynamics suite of programs capable of handling all marine and offshore analysis issues.

ACKNOWLEDGEMENTS

This work was supported in part by the American Bureau of Shipping and by the Office of Naval Research (ONR Grant N00014-13-1-0756). The authors would like to thank Dr. Richard Korpus for sharing his insight on ship performance and Dr. Robert Brizzolara for continuing his support.

REFERENCES

MA Abkowitz. *Stability and Motion Control of Ocean Vehicles*. MIT Press, Cambridge, MA, 1969.

Peter Boese. *Eine einfache Methode zur Berechnung der Widerstandserh{ö}hung eines Schiffes im Seegang*, volume 17. Inst. f{ü}r Schiffbau der Univ. Hamburg, 1970.

Frank Chou, John Chianis, and Xinyu Zhang. SELF INSTALLED SINGLE COLUMN FLOATER. In *23rd International Conference on Offshore Mechanics and Arctic Engineering*, Vancouver, 2004.

T Duarte and a J N a Sarmento. Effects of Second-Order Hydrodynamic Forces on Floating Offshore Wind Turbines. In *32nd ASME Wind Energy Symposium*, number January, National Harbor, Maryland, 2014. American Institute of Aeronautics and Astronautics.

OM Faltinsen, KJ Minsaas, N Liapis, and SO Skjørdal. Prediction of resistance and propulsion of a ship in a seaway. In *Proc. 13th Symposium on Naval Hydrodynamics*, 1980.

Jeffrey Falzarano, Abhilash Somayajula, and Robert Seah. An overview of the prediction methods for roll damping of ships. *Ocean Systems Engineering*, 5(2):55–76, 2015.

Amitava Guha. *Development of a Computer Program for Three Dimensional Frequency Domain Analysis of Zero Speed First Order Wave Body Interaction*. Master thesis, Texas A&M University, College Station, TX, 2012.

Amitava Guha. *Development and Application of a Potential Flow Computer Program: Determining First and Second Order Wave Forces at Zero and Forward Speed in Deep and Intermediate Water Depth*. Phd dissertation, Texas A&M University, College Station, TX, 2016.

Amitava Guha and Jeffrey Falzarano. Estimation of Hydrodynamic Forces and Motion of Ships with Steady Forward Speed. *Accepted in International Shipbuilding Progress*, pages 1–38, 2015a.

Amitava Guha and Jeffrey Falzarano. The effect of hull emergence angle on the near field formulation of added resistance. *Ocean Engineering*, 105(1):10–24, sep 2015b. ISSN 00298018. doi: 10.1016/j.oceaneng.2015.06.012.

Amitava Guha and Jeffrey Falzarano. Application of Multi Objective Genetic Algorithm in Ship Hull Optimization. *Ocean Systems Engineering*, 5(2):91–107, 2015c. doi: 10.12989/ose.2015.5.2.091.

Amitava Guha and Jeffrey M. Falzarano. Development of a Computer Program for Three Dimensional Analysis of Zero Speed First Order Wave Body Interaction in Frequency Domain. In *Proceedings of the ASME 2013 32nd International Conference on Ocean, Offshore and Arctic Engineering*, pages 1–9, Nantes, France, jun 2013. ASME. ISBN 978-0-7918-5539-3. doi: 10.1115/OMAE2013-11601.

Amitava Guha, Abhilash Somayajula, and Jeffrey M. Falzarano. Analysis of Causeway Ferry Dynamics for Safe Operation of Improved Navy Lighterage System. In *Proceedings of the 13th International Ship Stability Workshop*, pages 1–8, Brest, 2013.

H a Haslum, Umoe Olje, and O M Faltinsen. Alternative Shape of Spar Platforms for Use in Hostile Areas. *Proceedings of Offshore Technology Conference*, pages 1–12, 1999. ISSN 01603663.

HA Haslum. *Simplified methods applied to nonlinear motion of spar platforms*. Doctorate dissertation, Norwegian University of Science and Technology, 2000.

Herbjørn Haslum. Various applications of spar platforms. *70 Years Anniversary Seminar for Professors Odd M. Faltinsen and Torgeir Moan*, 2004.

J L Hess and A M Smith. Calculation of non-lifting potential flow about arbitrary three-dimensional bodies. *Journal of Ship Research*, 8(3):22–44, 1964.

Edward Huang, Shankar Bhat, Yong Luo, and Jun Zou. Evaluation of Dry Tree Platform Concepts. *Offshore Technology Conference*, pages 1–13, 2000. ISSN 01603663. doi: 10.4043/11899-MS.

R.P. Huijsmans, R.H.M. and Dallinga. Non-linear Ship Motions in Shallow Water. In *Ship and platform motion symposium*, 1983.

Yoshiho Ikeda, Yoji Himeno, and Nori Tanaka. A Prediction Method for Ship Roll Damping. Technical report, Department of Naval Architecture, University of Osaka Prefecture, 1978.

F John. On the motion of floating bodies I. *Communications on pure and applied mathematics*, 2(1):13–57, 1949.

F John. On the motion of floating bodies II. Simple harmonic motions. *Communications on pure and applied mathematics*, 3(1): 45–101, 1950.

C H Lee. WAMIT User Manual. Technical report, WAMIT, Inc., Chestnut Hill, MA, USA, 2013.

EM Lewandowski. *The dynamics of marine craft: maneuvering and seakeeping*. World Scientific, Singapore, 2004.

Lin Li. *Numerical seakeeping Predictions of Shallow Water Effect on Two Ship Interactions in Waves*. Phd dissertation, Dalhousie University, 2001.

C. M. Linton. Rapidly convergent representations for Green' functions for Laplace' equation. *Proceedings of the Royal Society A: Mathematical, Physical and Engineering Sciences*, 455(1985):1767–1797, 1999. ISSN 1364-5021. doi: 10.1098/rspa.1999.0379.

Yingyi Liu, Hidetsugu Iwashita, and Changhong Hu. A calculation method for finite depth free-surface green function. *International Journal of Naval Architecture and Ocean Engineering*, 7:375–389, 2015.

Hajime Maruo. Wave Resistance of a Ship in Regular Head Seas. *Bulletin of the Faculty of Engineering, Yokohama National University*, 9(March), 1960.

Hisham Moideen, Jeffrey M. Falzarano, and Abhilash Sharma Somayajula. Parametric roll of container ships in head waves. *Ocean Systems Engineering*, 2(4):239–255, dec 2012. ISSN 2093-6702. doi: 10.12989/ose.2012.2.4.239.

Hisham Moideen, Abhilash Somayajula, and Jeffrey M. Falzarano. Parametric Roll of High Speed Ships in Regular Waves. In *Proceedings of ASME 2013 32nd International Conferences on Ocean, Offshore and Arctic Engineering*, volume 5, page V005T06A095. ASME, jun 2013. ISBN 978-0-7918-5539-3. doi: 10.1115/OMAE2013-11602.

Hisham Moideen, Abhilash Somayajula, and Jeffrey M Falzarano. Application of Volterra Series Analysis for Parametric Rolling in Irregular Seas. *Journal of Ship Research*, 58(2):1–9, 2014. ISSN 15420604. doi: http://dx.doi.org/10.5957/JOSR.58.2.130047.

V. J. Monacella. The Disturbance Due to a Slender Ship Oscillating in Waves in a Fluid of Finite Depth. *Journal of Ship Research*, 10(4):242–252, 1966.

J.N. N. Newman. Numerical solutions of the water-wave dispersion relation. *Applied Ocean Research*, 12(1):14–18, jan 1990. ISSN 01411187. doi: 10.1016/S0141-1187(05)80013-6.

Orcina. OrcaFlex Manual v10.0a. Technical report, Orcina Ltd., Ulverston, Cumbria, UK, 2015.

M. K. Pidcock. The Calculation of Green's Functions in Three Dimensional Hydrodynamics Gravity Wave Problem. *International journal for numerical methods in fluids*, 5:891–909, 1985.

J.A. Pinkster. Mean And Low Frequency Wave Drifting Forces On Floating Structures. *Ocean engineering*, 6(1):593–615, 1979.

Abhilash Somayajula. *Ship Roll Dynamics in Irregular Seas*. Phd dissertation proposal, Texas A&M University, 2015.

Abhilash Somayajula and Jeffrey Falzarano. Large-amplitude time-domain simulation tool for marine and offshore motion prediction. *Marine Systems & Ocean Technology*, 10(1):1–17, 2015a. doi: 10.1007/s40868-015-0002-7.

Abhilash Somayajula and Jeffrey M. Falzarano. Non-linear Dynamics of Parametric Roll of Container Ship in Irregular Seas. In *Proceedings of ASME 2014 33rd International Conferences on Ocean, Offshore and Arctic Engineering*, pages 1–10, San Francisco, 2014a. ISBN 9780791845493. doi: 10.1115/OMAE2014-24186.

Abhilash Somayajula and Jeffrey M Falzarano. Non-Gaussian Analysis Methods for Planing Craft Motion. *International Journal of Ocean Systems Engineering*, 4(4):293–308, 2014b.

Abhilash Somayajula, Amitava Guha, Jeffrey Falzarano, Ho-hwan Chun, and Kwang Hyo Jung. Added resistance and parametric roll prediction as a design criteria for energy efficient ships. *Ocean Systems Engineering*, 4(2):117–136, jun 2014. ISSN 2093-6702. doi: 10.12989/ose.2014.4.2.117.

Abhilash Sharma Somayajula and Jeffrey M Falzarano. Validation of Volterra Series Approach for Modelling Parametric Rolling of Ships. In *34th International Conference on Ocean, Offshore and Arctic Engineering*, St. John's, Newfoundland, Canada, 2015b.

J V Wehausen and E V Laitone. Surface waves. *Encyclopedia of Physics*, 9:446–815, 1960.

J. D. Wheeler. Method for Calculating Forces Produced by Irregular Waves. *Journal of Petroleum Technology*, 249:359–367, 1970.